J. Fluid Mech. (2004), *vol.* 502, *pp.* 65–87. © 2004 Cambridge University Press
DOI: 10.1017/S0022112003007249 Printed in the United Kingdom

Fractal-generated turbulence

By B. MAZZI[1] AND J. C. VASSILICOS[2]

[1]Department of Applied Mathematics and Theoretical Physics, University of Cambridge, Centre for Mathematical Sciences, Wilberforce Road, Cambridge, CB3 0WA, UK

[2]Department of Aeronautics, Imperial College of Science Technology and Medicine, London, UK

(Received 29 January 2003 and in revised form 2 October 2003)

A model fractal forcing for direct numerical simulations (DNS) of stationary, homogeneous and isotropic turbulence is proposed. The power spectrum of this forcing is a power-law function of wavenumber with a positive exponent that is an increasing function of D_f, the fractal dimension of the fractal stirrer. The following results are obtained for DNS turbulence subjected to fully self-similar fractal forcing of fractal dimension D_f. (i) The Taylor and Kolmogorov microscales are proportional to each other and to the smallest length scale of the fractal forcing. (ii) The integral length scale is much smaller than the size L_b of the DNS box and a decreasing function of the extent of the fractal forcing range because fractal forcing generates very irregular velocity fields. (iii) In qualitative (but not quantitative) agreement with renormalization group (RG) theories of turbulence, higher values of D_f lead to increased energy at the highest wavenumbers. (iv) The energy and energy input rate spectra and the inter-scale energy transfer $T(k)$ all scale with the turbulence r.m.s. velocity u' and the Taylor microscale λ. (v) More than 80% of the total dissipation occurs in the fractal forcing range of scales which extends from L_b to about one to two times the Taylor microscale. In that range, $T(k)$ is negligible. (vi) $\lambda \sim \nu/u'$ (where ν is the kinematic viscosity), the kinetic energy dissipation rate per unit mass $\epsilon \sim u'^3/\lambda \sim u'^4/\nu$ and the velocity derivative skewness S is independent of Reynolds number in the limit where the Reynolds number and the fractal forcing range are increased together. (vii) The intermediate eigenvalue of the strain rate tensor is on average positive, and the negligible values of $T(k)$ in the fractal forcing range are accompanied by lower values of S and a significant reduction in local compression by comparison to turbulence forced only at the large scales. (viii) The geometrical alignments between vorticity, strain rate tensor eigenvectors and vortex stretching vector are qualitatively as in turbulence forced only at the large scales but significantly weakened. (ix) The p.d.f.s of velocity increments are approximately, though not exactly, Gaussian at all scales between the Kolmogorov and integral length scales. A few preliminary DNS results are also given for the case of turbulence generated by a fractal forcing that is discretely, as opposed to fully, self-similar.

1. Introduction

The essence of the problem involved in understanding and predicting turbulent flows revolves around three interrelated aspects of high-Reynolds-number turbulence: (i) the existence of a broad continuous range of excited length and time scales; (ii) the nonlinear transfer of energy between these scales; and (iii) the Reynolds number independence of turbulent kinetic energy dissipation in the limit of very large Reynolds numbers.

https://doi.org/10.1017/S0022112003007249 Published online by Cambridge University Press

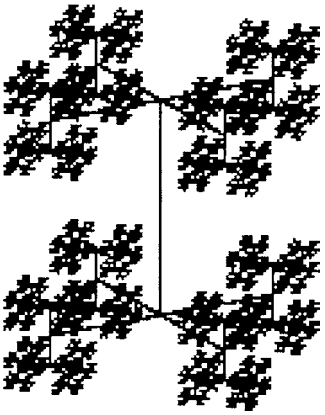


FIGURE 1. Sketch of the fractal object used by Queiros-Conde & Vassilicos (2001) and Staicu *et al.* (2003).

For a wide variety of turbulent flows, predictions and experimental investigations have been based on assumptions of independence from inner and outer scales in certain intermediate ranges (inertial range in homogeneous turbulence, overlap region in turbulent boundary layers and turbulent pipe flows), locality of interscale energy transfer in such intermediate ranges, Reynolds number independence of dissipation, scale-invariance and self-similarity and even unversality. In one way or another these assumptions lead to similarity scalings and power-law forms of energy spectra and structure functions both in wall-bounded turbulent flows and in homogeneous turbulence. Some of these power-law dependencies of energy spectra on wavenumber and of structure functions on separation distance involve non-integer powers which imply, as noted by Onsager (1949; see also Frisch 1995) and later by Hunt & Vassilicos (1991) (but see also Perry, Henbest & Chong 1986), that realizations of the turbulence must have a near-singular spatial structure which is more complicated than mere well-separated discontinuities (in the form of little shear layers, for example). This near-singular turbulent flow structure must have aspects of fractal and/or spiral geometry (Hunt & Vassilicos 1991; Vassilicos & Hunt 1991) and a significant number of theoretical papers were written starting with the pioneering works of Novikov (1970), Mandelbrot (1974), Frisch, Sulem & Nelkin (1978), Lundgren (1982) and Parisi & Frisch (1985) attempting to account for many turbulence properties and phenomena in terms of this underlying fractal and/or spiral flow structure (and extensions to multifractals and multispirals were also developed in the 1980s and 1990s – see Frisch 1995; Vassilicos 1992).

The similarity in the dynamics and geometry of the turbulence between different scales of motion prompted the use of renormalization group (RG) techniques for solving Navier–Stokes turbulence (see Lesieur 1990; McComb 1990; Frisch 1995; Smith & Woodruff 1998). Central to this approach is the use of a power-law forcing in wavenumber space (which can be an increasing as well as a decreasing function of wavenumber) to establish the self-similarity necessary to use RG. Most turbulent flows in the laboratory are not forced in such a way, with the exception of recent experiments by Queiros-Conde & Vassilicos (2001) and Staicu *et al.* (2003) who used fractal objects (see figure 1) to generate turbulence in a wind tunnel. As argued by Mazzi, Okkels & Vassilicos (2002) on the basis of a rough estimate of the drag force on the fractal stirrer, fractal stirrers force the turbulence over the entire range of their

https://doi.org/10.1017/S0022112003007249 Published online by Cambridge University Press

self-similar length-scales in a way that mimics a power-law forcing in wavenumber space. The other advantage of this laboratory experiment is in its attempt to directly tamper with the multiple-scale fractal and/or spiral geometry of the turbulence which, as argued in the preceding paragraph, is so closely linked to its multiple-scale dynamics and spectral scalings.

The major result of the RG approach to turbulence has been to show that, when the incompressible three-dimensional Navier–Stokes equations are subjected to a stochastic forcing with a power spectrum proportional to k^{1-y} (where k stands for wavenumber and y is a scaling parameter between 0 and 4) then the energy spectrum of the turbulence scales as $k^{1-2y/3}$ (see Lesieur 1990; McComb 1990; Frisch 1995; Smith & Woodruff 1998 and references therein). The RG forcing is delta-correlated in time and wavenumber space, and direct numerical simulations (DNS) of the Navier–Stokes equations so forced (Sain, Pandit & Pandit 1998) have confirmed the $k^{-5/3}$ form of the energy spectrum when $y = 4$ as well as its $k^{1-2y/3}$ form for $y = 1, 2, 3$, and have suggested that the spectrum keeps its $-5/3$ scaling for $y > 4$.

Numerical integrations of a GOY shell model modified for the power spetrum of the forcing to scale as k^{1-y} have resulted in a turbulence energy spectrum which scales as $k^{-5/3}$ for all y greater or equal to a threshold value y_c and which is progressively shallower as y decreases below y_c (Mazzi *et al.* 2002). This is in qualitative agreement with the RG predictions and the DNS calculations of Sain *et al.* (1998) in as far as the energy spectrum becomes shallower as y decreases below a threshold value y_c and takes the Kolmogorov form $k^{-5/3}$ for $y \geqslant y_c$. However, there is strong quantitative disagreement in the values of y_c. When the forcing of the turbulence is delta-correlated in time and wavenumber space, as in the RG analyses described in Lesieur (1990), McComb (1990), Frisch (1995), Smith & Woodruff (1998) and as in the DNS computations of Sain *et al.* (1998), then we might expect $y_c = 4$. In the GOY model integrations of Mazzi *et al.* (2002), the forcing is time-independent and various wavenumber space correlations have been tried, leading to values of y_c between $1/3$ and about 0.

The inevitable constraining assumptions of the shell model and of the delta-correlated stochastic forcing prompts the present approach to fractal-forced turbulence by DNS. The forcing used here has a power-law dependence on wavenumber as expected in laboratory experiments of fractal-forced turbulence (Mazzi *et al.* 2002) and as used in the RG approaches to turbulence (see Lesieur 1990; McComb 1990; Frisch 1995; Smith & Woodruff 1998), in the DNS computations of Sain *et al.* (1998) and in the GOY model integrations of Mazzi *et al.* (2002). The only other constraints that we impose on the forcing are incompressibility and stationarity at every time step. In particular, our forcing is not stochastic and not delta-correlated in time and wavenumber-space. In this paper, we detail the fractal forcing of our DNS and its implementation (see § 2) and report the results of our study of statistically stationary fractal-forced turbulence.

In § 3, we present the effect of a fully self-similar fractal forcing on spectra and bulk properties of the turbulence including the integral length scale. In § 4, we describe the scaling of the energy spectrum, in § 5 the scaling of the inter-scale energy transfer $T(k)$ and of the energy input rate spectrum $\mathscr{F}(k)$ and in § 6 the scaling of the energy dissipation rate ϵ and the Taylor microscale. Section 7 is dedicated to the relation between skewness and transfer and the alignments between vorticity, the eigenvectors of the strain rate tensor and the vortex stretching vector. In § 8, we study the p.d.f.s of longitudinal velocity increments δu_r. In § 9 we present a few results on turbulence generated by a discretely self-similar fractal forcing, and conclude in § 10.

https://doi.org/10.1017/S0022112003007249 Published online by Cambridge University Press

2. Fractal forced DNS

2.1. *The forcing scheme*

We use a pseudospectral DNS code which solves the Fourier transformed incompressible Navier–Stokes equations

$$\left(\frac{\partial}{\partial t}+\nu k^2\right)\hat{\boldsymbol{u}}=-\boldsymbol{P}\widehat{\boldsymbol{\omega}\wedge\boldsymbol{u}}+\boldsymbol{P}\hat{\boldsymbol{F}}, \tag{2.1}$$

where

$$P_{ij}=\delta_{ij}-\frac{k_i k_j}{k^2} \tag{2.2}$$

is the projection tensor onto the plane normal to the wavevector $\boldsymbol{k}$, $\hat{\boldsymbol{u}}$ is the Fourier transform of the velocity field, $k=|\boldsymbol{k}|$, ν is the kinematic viscosity, $\hat{\boldsymbol{F}}(\boldsymbol{k},t)$ is the Fourier transform of the forcing term and $\widehat{\boldsymbol{\omega}\wedge\boldsymbol{u}}$ is the Fourier transform of the vector product of the vorticity and velocity fields.

We calculate $\hat{\boldsymbol{u}}(\boldsymbol{k},t+\Delta t)$ from $\hat{\boldsymbol{u}}(\boldsymbol{k},t)$ as follows

$$\hat{\boldsymbol{u}}(\boldsymbol{k},t+\Delta t)=\hat{\boldsymbol{u}}_{NS}(\boldsymbol{k},t+\Delta t)+\Delta t\,\boldsymbol{P}\hat{\boldsymbol{F}}, \tag{2.3}$$

where

$$\hat{\boldsymbol{u}}_{NS}(\boldsymbol{k},t+\Delta t)\equiv\hat{\boldsymbol{u}}(\boldsymbol{k},t)+\Delta t(-\nu k^2\hat{\boldsymbol{u}}-\boldsymbol{P}\widehat{\boldsymbol{\omega}\wedge\boldsymbol{u}}), \tag{2.4}$$

and Δt is the time interval over one time step.

The fractal forcing is simulated in the following way:

$$\boldsymbol{P}\hat{\boldsymbol{F}}=(kL_b)^{\beta}a_k f\boldsymbol{e}, \tag{2.5}$$

where f is a scalar independent of $\boldsymbol{k}$ and $\boldsymbol{e}=\boldsymbol{e}(\boldsymbol{k},t)$ is a unit vector; the coefficient a_k is equal to 1 or 0 according to whether k is a forced or unforced wavenumber. The fractal nature of the forcing is modelled by the power law $(kL_b)^{\beta}$ where L_b is the largest forced length scale (and in fact also the size of our DNS periodic box) and β is a scaling exponent dictated by the design and fractal dimension D_f of the fractal stirrer or obstacle (we use here this exponent β instead of the exponent y that is customary in the RG literature). We might expect, in general, on the grounds that drag is proportional to surface area, that $|\boldsymbol{P}\hat{\boldsymbol{F}}|\sim k^{-2}N(k^{-1})$ or $|\boldsymbol{P}\hat{\boldsymbol{F}}|\sim k^{-1}N(k^{-1})$ according to whether the surface is such that its area scales with k^{-2} or k^{-1} (see the Appendix): here, $N(k^{-1})\sim k^{D_f}$ is the fractal box-counting number of boxes of size k^{-1} covering the surface of the fractal obstacle. This gives $\beta=D_f-2$ or $\beta=D_f-1$.

A relation between β and D_f estimated for a specific fractal design similar to that in figure 1 has been given in Mazzi *et al.* (2002) and is in satisfactory agreement with $\beta=D_f-2$ except that the finite nature of the fractal objects implies, in practice, that β is in fact slightly smaller than D_f-2 (see Queiros-Conde & Vassilicos (2001) and Mazzi *et al.* (2002)). In the Appendix, we present the case of the Koch pole where $\beta=D_f-1$.

From equations (2.3) and (2.5) we obtain

$$\sum_{\boldsymbol{k}}|\hat{\boldsymbol{u}}(\boldsymbol{k},t+\Delta t)|^2=\sum_{\boldsymbol{k}}|\hat{\boldsymbol{u}}_{NS}(\boldsymbol{k},t+\Delta t)|^2 + 2f\Delta t\sum_{\boldsymbol{k}}\hat{\boldsymbol{u}}_{NS}(\boldsymbol{k},t+\Delta t)\cdot\boldsymbol{e}a_k(kL_b)^{\beta}+f^2(\Delta t)^2\sum_{\boldsymbol{k}}a_k^2(kL_b)^{2\beta}. \tag{2.6}$$

https://doi.org/10.1017/S0022112003007249 Published online by Cambridge University Press

Defining $2\Delta E \equiv \sum_{\boldsymbol{k}} |\hat{\boldsymbol{u}}(\boldsymbol{k}, t)|^2 - \sum_{\boldsymbol{k}} |\hat{\boldsymbol{u}}_{NS}(\boldsymbol{k}, t+\Delta t)|^2$, statistical stationarity is achieved when

$$f\Delta t \sum_{\boldsymbol{k}} \hat{\boldsymbol{u}}_{NS}(\boldsymbol{k}, t+\Delta t)\cdot \boldsymbol{e} a_k (kL_b)^{\beta} + \tfrac{1}{2}(\Delta t)^2 f^2 \sum_{\boldsymbol{k}} a_k^2 (kL_b)^{2\beta} = \Delta E. \tag{2.7}$$

The unit vector $\boldsymbol{e}(\boldsymbol{k})$ in (2.5) must satisfy the constraints

$$|\boldsymbol{e}|^2 = 1,$$
$$\boldsymbol{k}\cdot\boldsymbol{e} = 0,$$
$$\boldsymbol{e}(-\boldsymbol{k}) = \boldsymbol{e}(\boldsymbol{k})^*,$$

because the fractal forcing should not affect the incompressible and real-valued nature of the velocity field. The most general form of $\boldsymbol{e}(\boldsymbol{k}, t)$ under these constraints is

$$\boldsymbol{e}(\boldsymbol{k}, t) = \alpha \frac{\hat{\boldsymbol{u}}(\boldsymbol{k}, t)}{|\hat{\boldsymbol{u}}(\boldsymbol{k}, t)|} + \gamma \frac{\boldsymbol{k}\wedge\hat{\boldsymbol{u}}(\boldsymbol{k}, t)}{|\boldsymbol{k}||\hat{\boldsymbol{u}}(\boldsymbol{k}, t)|}, \tag{2.8}$$

where

$$\alpha^2 + \gamma^2 = 1, \tag{2.9}$$

and

$$\alpha^* = \alpha,$$
$$\gamma^* = -\gamma.$$

The last condition requires that α be purely real and γ purely imaginary. Substituting the form (2.8) of the vector $\boldsymbol{e}$ into (2.7), we obtain

$$f\alpha = \frac{(\Delta E/\Delta t) - \tfrac{1}{2}\Delta t f^2 \sum_{\boldsymbol{k}} a_k^2 (kL_b)^{2\beta}}{\sum_{\boldsymbol{k}} |\hat{\boldsymbol{u}}_{NS}(\boldsymbol{k}, t+\Delta t)| a_k (kL_b)^{\beta}}. \tag{2.10}$$

In the limit $\Delta t \to 0$ and replacing $\Delta E/\Delta t$ by ϵ, the kinetic energy dissipation per unit mass (2.10) tends to

$$f\alpha = \frac{\epsilon}{\sum_{\boldsymbol{k}} |\hat{\boldsymbol{u}}_{NS}(\boldsymbol{k}, t+\Delta t)| a_k (kL_b)^{\beta}} + O(\Delta t). \tag{2.11}$$

Note that $f\alpha \sum_{\boldsymbol{k}} |\hat{\boldsymbol{u}}_{NS}(\boldsymbol{k}, t+\Delta t)| a_k (kL_b)^{\beta}$ is equal to $\frac{1}{2}\sum_{\boldsymbol{k}} [(\boldsymbol{P}\hat{\boldsymbol{F}})^* \cdot \hat{\boldsymbol{u}}_{NS} + (\boldsymbol{P}\hat{\boldsymbol{F}})\cdot \hat{\boldsymbol{u}}_{NS}^*]$ which is the total energy input rate, so that (2.11) simply expresses, at first order, that stationarity of the turbulence requires the balance between energy input rate and dissipation rate ϵ.

The determination of the fractal forcing $\boldsymbol{P}\hat{\boldsymbol{F}}$ requires formulae for $f\alpha$ and $f\gamma$ which can be readily obtained from (2.11), (2.9) and from the requirement that the $O(\Delta t)$ correction in (2.11) should be as small as possible. We note from (2.10) that this $O(\Delta t)$ correction vanishes in the limit $f \to 0$ whilst keeping $f\alpha$ constant (by taking the limit $\alpha \to \infty$ at the same time), and that $f\gamma = \pm \mathrm{i} f\alpha$ from (2.9) in that same limit. Here we chose $f\gamma = \mathrm{i} f\alpha$.

Hence,

$$\boldsymbol{P}\hat{\boldsymbol{F}} = (kL_b)^{\beta} a_k f\alpha \left[\frac{\hat{\boldsymbol{u}}(\boldsymbol{k}, t)}{|\hat{\boldsymbol{u}}(\boldsymbol{k}, t)|} + \mathrm{i} \frac{\boldsymbol{k}\wedge\hat{\boldsymbol{u}}(\boldsymbol{k}, t)}{|\boldsymbol{k}||\hat{\boldsymbol{u}}(\boldsymbol{k}, t)|} \right], \tag{2.12}$$

https://doi.org/10.1017/S0022112003007249 Published online by Cambridge University Press

where $f\alpha$ is obtained from (2.11) without the $O(\Delta t)$ correction. This fully determines the fractal power law forcing at every time step and wavenumber $\boldsymbol{k}$ provided we input the values of β, L_b and a_k as well as the largest wavenumber K_F of the fractal forcing. The ratio of the largest to the smallest fractal forced lengthscales is represented by $K_F L_b$ and $a_k = 0$ for $k > K_F$. In this paper, we mainly deal with the case of a fully self-similar forcing where

$$a_k = \begin{cases} 1 & \text{for } k < K_F, \\ 0 & \text{for } k > K_F, \end{cases} \tag{2.13}$$

but in §9, we also briefly explore the case of a fractal forcing with discrete self-similarity such that

$$a_k = \begin{cases} 1 & \text{for } k = (2\pi/L_b)\sigma^n, \\ 0 & \text{elsewhere,} \end{cases} \tag{2.14}$$

where σ is a parameter larger than 1 characteristic of the discrete forcing, n is an integer, $n = 0, \ldots, n_F$, and n_F is defined by $(2\pi/L_b)\sigma^{n_F} \leqslant K_F < (2\pi/L_b)\sigma^{n_F+1}$.

We find that DNS of turbulence subjected to fully self-similar forcing over a wide range of scales is numerically stable for all the values of β that we tried ($0.1 \leqslant \beta \leqslant 0.7$), provided that $3K_F/2$ is smaller or approximately equal to the largest resolved wavenumber k_{max}. Hence, given a resolution $k_{max}\eta > 1$ (where $\eta \equiv (\nu^3/\epsilon)^{1/4}$), the largest possible range of scales subjected to fully self-similar forcing is obtained for $K_F \approx 2/3k_{max}$.

2.2. *The data*

The initial conditions are random with an energy spectrum set as

$$E(k, t = 0) \sim \exp(-b(kL_b/2\pi)^2), \tag{2.15}$$

with $b > 0$. This ensures that all the energy is initially concentrated at the largest scales. Statistics were taken once the properties of the flow (length scales, skewness, flatness…) reached a constant value.

In tables 1 and 2 we list the main parameters and characteristics of the DNS performed for the turbulence subjected to fully self-similar forcing. Runs XIV and XV are tests of the forcing scheme presented in §2.1.

In tables 1 and 2, N is the number of grid points, λ is the Taylor-microscale, Re_λ is the Taylor-based Reynolds number, Re_{L_b} is the Reynolds number based on the box size L_b, L is the integral length scale, τ is the eddy-turnover time defined by $\tau = L/u'$, $CFL = u_{max}N\Delta t/2\pi$, $S = -\langle(\partial u/\partial x)^3\rangle/\langle(\partial u/\partial x)^2\rangle^{3/2}$ and $F = \langle(\partial u/\partial x)^4\rangle/\langle(\partial u/\partial x)^2\rangle^2$ where u is the velocity field component in the x-direction and the brackets $\langle\cdots\rangle$ denote time averaging; ϵ_F is the fraction of the dissipation integral contributed by wavenumbers larger than the forcing cutoff K_F, namely

$$\epsilon_F = \frac{\displaystyle\int_{K_F}^{\infty} k^2 E(k)\,\mathrm{d}k}{\displaystyle\int_0^{\infty} k^2 E(k)\,\mathrm{d}k}, \tag{2.16}$$

where $E(k)$ is the energy spectrum of the turbulence. Note the striking result that only between 9% and 17% of the total dissipation occurs at wavenumbers larger than K_F in fractal-forced turbulence. The last two runs 'CF' are taken from Flohr (1999) as examples of DNS turbulence forced only at the large scales by a different forcing scheme for comparison with runs XIV and XV, respectively. $K_F \sim 2/3k_{max}$ for

https://doi.org/10.1017/S0022112003007249 Published online by Cambridge University Press

Run	N	$K_F L_b$	β	L/L_b	Re_λ	Re_{L_b}	CFL	Duration/τ	τ
I	64	94.2	0.1	0.110	8.9	188	0.38	26.09	0.69
II	64	94.2	0.33	0.079	7.5	188	0.40	36.00	0.50
IIb	96	94.2	0.33	0.087	7.6	188	0.43	14.8	0.54
III	64	94.2	0.60	0.065	6.7	188	0.39	43.90	0.41
IV	96	188.4	0.1	0.076	8.1	314	0.44	25.00	0.48
V	96	188.4	0.2	0.070	7.4	314	0.42	27.27	0.44
VI	96	188.4	0.33	0.059	6.7	314	0.45	32.43	0.37
VII	96	188.4	0.45	0.046	6.2	314	0.43	41.38	0.29
VIII	96	188.4	0.60	0.041	5.8	314	0.43	46.15	0.26
IX	96	188.4	0.70	0.037	5.6	314	0.43	52.17	0.23
X	128	263.8	0.33	0.051	6.8	432	0.6	37.50	0.32
XI	192	376.8	0.1	0.060	8.3	628	0.97	23.68	0.38
XII	192	376.8	0.33	0.033	6.7	628	0.96	57.14	0.21
XIII	192	376.8	0.6	0.025	5.9	628	0.99	56.25	0.16
XIV	96	12.5	0.6	0.175	41.0	314	0.34	10.91	1.1
XV	192	12.5	0.6	0.15	63.4	628	0.38	16.84	0.95
CF	96	12.5	class	0.19	49		0.40		1.19
CF	192	12.5	class	0.18	82		0.36		1.13

TABLE 1. DNS parameters and data 1.

Run	N	η/λ	λ/L	η/L	$k_{max}\eta$	$K_F\lambda$	ϵ_F	S	F
I	64	0.16	0.43	0.07	1.52	4.46	0.12	0.34	3.41
II	64	0.19	0.49	0.09	1.39	4.65	0.15	0.32	3.23
IIb	96	0.18	0.49	0.09	2.12	3.83	0.71	0.33	3.33
III	64	0.19	0.54	0.11	1.32	3.64	0.17	0.32	3.19
IV	96	0.18	0.33	0.06	1.30	4.72	0.09	0.29	3.29
V	96	0.19	0.33	0.06	1.25	4.35	0.10	0.28	3.27
VI	96	0.20	0.36	0.07	1.18	4.80	0.12	0.27	3.20
VII	96	0.20	0.42	0.08	1.14	3.63	0.13	0.26	3.15
VIII	96	0.21	0.44	0.09	1.11	3.40	0.14	0.24	3.12
IX	96	0.21	0.52	0.11	1.08	3.62	0.15	0.24	3.12
X	128	0.19	0.30	0.06	1.14	4.62	0.11	0.25	3.18
XI	192	0.17	0.22	0.04	1.32	4.85	0.09	0.29	3.31
XII	192	0.20	0.31	0.06	1.18	4.80	0.12	0.26	3.20
XIII	192	0.21	0.35	0.07	1.11	3.30	0.14	0.25	3.14
XIV	96	0.08	0.55	0.04	2.1	1.20	0.84	0.52	4.00
XV	192	0.06	0.47	0.03	2.62	0.88	0.92	0.49	4.40
CF	96	0.07	0.52	0.04	2.01	1.24		0.48	4.17
CF	192	0.06	0.38	0.02	2.19	0.86		0.46	4.94

TABLE 2. DNS parameters and data 2.

runs IV to XIII and $K_F \sim 1/2k_{max}$ for runs I, II, III. Run IIb was made to check numerical convergence, i.e. it was run with the same parameters as II, but at higher resolution and produced the same results.

Figure 2(*a*) shows that our forcing does indeed produce a stationary state within about 10 turnover times: the Taylor-based Reynolds number Re_λ plotted versus t/τ eventually reaches a non-fluctuating constant value. The total energy of our simulated velocity field is in fact a non-fluctuating constant for all time (figure 2*b*). It is worth noting that the delta-correlated stochastic power-law forcing of the DNS of Sain *et al.* (1998) leads to a Taylor-based Reynolds number that is strongly fluctuating in time.

https://doi.org/10.1017/S0022112003007249 Published online by Cambridge University Press

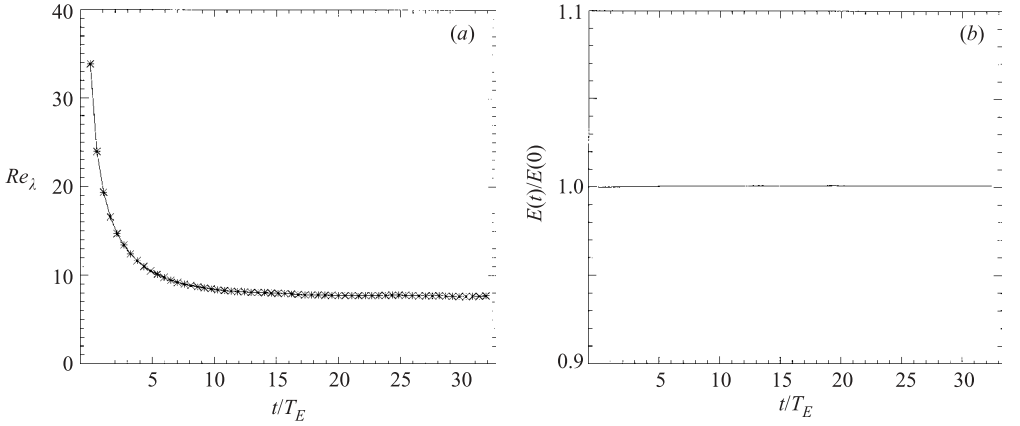


FIGURE 2. Stationarity: (*a*) the Taylor-based Reynolds number Re_λ plotted versus non-dimensional time t/τ (*b*) the total energy non-dimensionalized by its initial value as a function of t/τ.

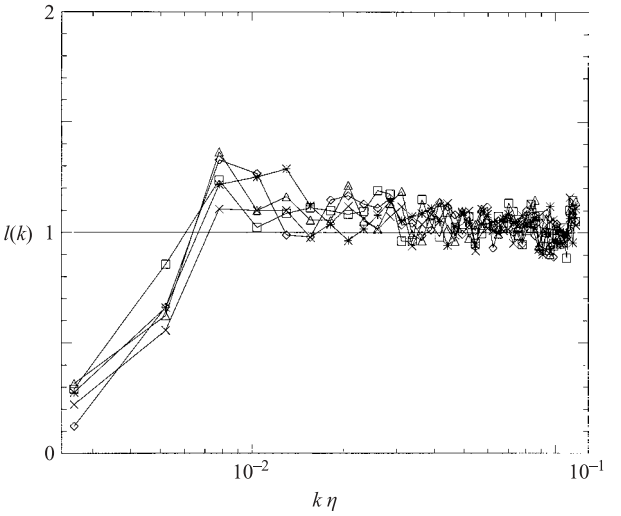


FIGURE 3. The isotropy coefficient for $N = 96$ (runs IV, V, VI, VII, VIII).

We tested our forcing scheme by running cases (runs XIV and XV in tables 1 and 2) where $a_k = 0$ for all $kL_b/2\pi > 2$ and $a_k \neq 0$ for $kL_b/2\pi = 1$ and 2 in (2.13) and obtained results in agreement with DNS forced at the large scales by other schemes (Kerr 1985; Eswaran & Pope 1988; Jiménez *et al.* 1993; Flohr 1999). In particular, the energy spectra $E(k)$, transfer spectra $T(k)$, integral, Taylor and Kolmogorov length scales, as well as the velocity derivative skewnesses and flatnesses S and F and isotropy coefficients are similar to DNS results obtained by other forcing schemes at similar Reynolds numbers (for example runs CF in tables 1 and 2 which were carried out in Flohr 1999).

3. Spectra and bulk properties

Our fully self-similar forcing produces a DNS turbulence which is stationary, homogenous and isotropic for all the values of β that we tried. In figure 3 we present

https://doi.org/10.1017/S0022112003007249 Published online by Cambridge University Press

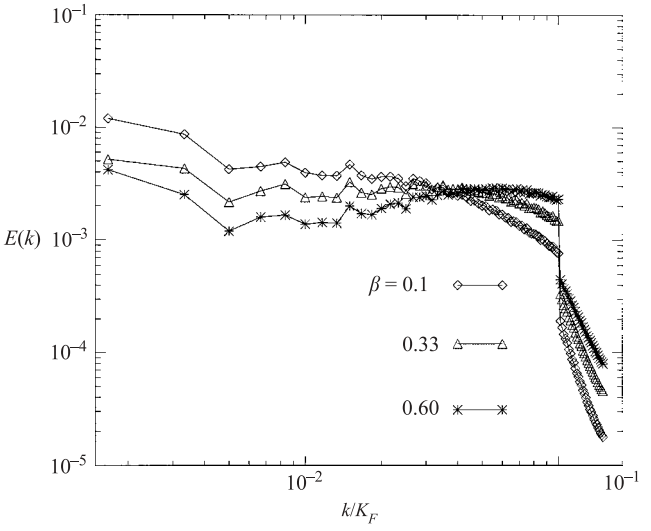


FIGURE 4. The energy spectrum for several values of β: the forcing is fully self-similar (runs XI, XII, XIII).

an example of a plot of the isotropy coefficient defined in equation (1) of Jiménez *et al.* (1993) which is representative of our findings. This coefficient takes values close to 1, which is indicative of isotropy, for nearly all scales except the very large ones which are comparable to the box size. We also find that the values of the velocity derivative skewness S and flatness F are significantly lower than for DNS turbulence with similar values of Re_{L_b}, but forced only at the large scales (see tables 1 and 2). Specifically, all the runs of fractal forced turbulence reported in tables 1 and 2 result in $0.24 < S < 0.34$ and $3.12 < F < 3.41$.

In figure 4, we plot the energy spectrum for several values of β (with a fully self-similar forcing).

One notices that the spectra differ slightly for different values of β and that they all intersect close to a particular wavenumber. This behaviour can be understood by examining the energy input rate spectrum

$$\mathscr{F}(k) = \frac{1}{2}\sum_{S(k)}[(\boldsymbol{P}\hat{\boldsymbol{F}})^* \cdot \hat{\boldsymbol{u}} + (\boldsymbol{P}\hat{\boldsymbol{F}}) \cdot \hat{\boldsymbol{u}}^*], \tag{3.1}$$

where the sum is over shells of radius k in wavevector space. This spectrum $\mathscr{F}(k)$, which we plot in figure 6 for different values of β, integrates to give the total energy input rate $\int \mathscr{F}(k)\,\mathrm{d}k$. There is a wavenumber where all the energy input spectra intersect in figure 6, and we have checked that this wavenumber is the one where the energy spectra also intersect. As might be expected, higher values of β correspond to more/less energy input rates and energies at wavenumbers above/below the intersection wavenumber. A similar observation was made in the context of RG theories of Navier–Stokes turbulence (see Lesieur 1990; McComb 1990; Frisch 1995; Smith & Woodruff 1998) and also by Mazzi *et al.* (2002) with their GOY model simulation who found that second-order structure functions are shallower for larger values of the grid's fractal dimension D_f (which corresponds to higher values of β above the intersection wavenumber) (see Mazzi *et al.* 2002). However, their structure functions correspond to energy spectra shallower than ours, whereas, compared to our

https://doi.org/10.1017/S0022112003007249 Published online by Cambridge University Press

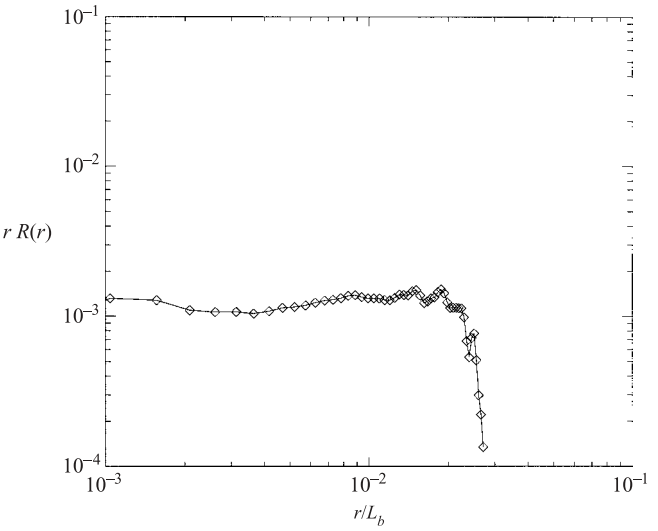


FIGURE 5. Plot of $r\,R(r)$ versus r/L_b where $R(r)$ is the velocity correlation.

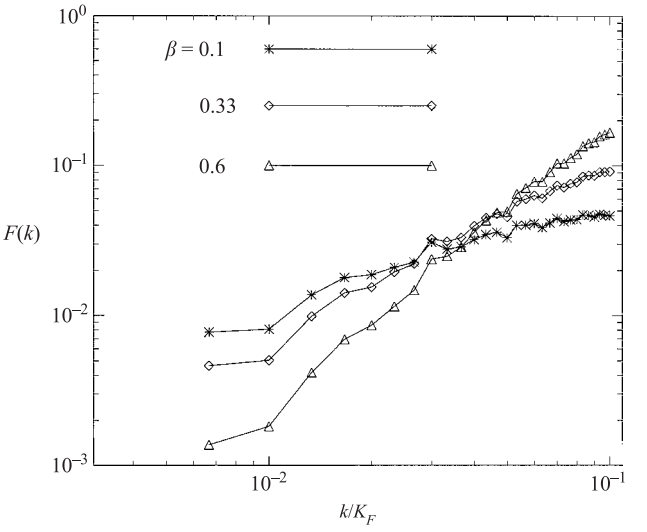


FIGURE 6. The energy input rate spectrum $\mathscr{F}(k)$ for different values of β (runs IV, VI, IX).

energy spectra, the RG energy spectra are significantly steeper increasing functions of wavenumber.

The energy is distributed across the scales much more equitably than when the forcing is limited to the large scales. A flat spectrum can be easily shown to lead to a velocity correlation† $R(r)$ scaling approximately as $\sim r^{-1}$; figure 5 shows the plot of $r\,R(r)$ revealing, as expected, a function very close to constant. The behaviour does change abruptly beyond the forcing cutoff K_F where the energy spectrum is a fast decreasing function of k. As a result of this increased energy at small scales, the

† Defined, for isotropic turbulence, as $R(r) = f(r) + 2g(r)$ with $u'^2 f(r) = \langle u_1(x)u_1(x+r)\rangle$ and $u'^2 g(r) = \langle u_1(x)u_2(x+r)\rangle$.

https://doi.org/10.1017/S0022112003007249 Published online by Cambridge University Press

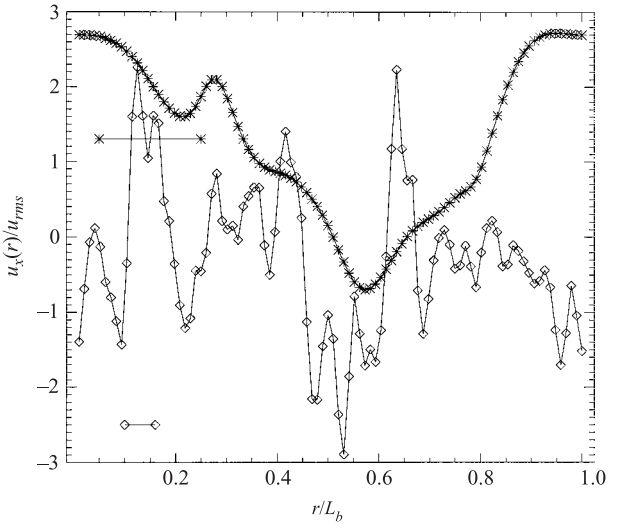


FIGURE 7. A plot of the velocity signal for a classical simulation (∗) and for a fractal forced one (◇). The value of the integral length scale L is also shown. In the fractal-forced case a simulation with $\beta = 0.1$ was used; no qualitative difference was encountered for other values of β.

integral length scale turns out to be much smaller than when the turbulence is only forced around the large scale L_b. In particular, L is found to be a decreasing function of $K_F L_b$, and in fact $L \ll L_b$ for all large enough values of $K_F L_b$ (see the values of L/L_b and $K_F L_b$ in tables 1 and 2). The integral length scale is an average over all length-scales $\sim 1/k$ given by (Batchelor 1953)

$$L = \tfrac{1}{2}\pi \int k^{-1} \frac{E(k)}{u'^2}\,\mathrm{d}k \tag{3.2}$$

where $3u'^2/2 = \int_0^\infty E(k)\,\mathrm{d}k$. An energy spectrum with a larger fraction of the energy at the smaller scales does therefore result in a smaller integral length scale L. To illustrate this point, we plot two examples of velocity signals obtained from fractal-forced and large-scale forced DNS of homogeneous isotropic turbulence (figure 7). The fractal-forced velocity signal is considerably more irregular than the large-scale forced velocity signal. This irregularity results in shorter correlation spans and the integral length-scale is therefore smaller.

4. Scaling of the energy spectrum

All our fractal-forced simulations are designed to have about the same values of $K_F\eta$, and a first result is that they turn out also to have about the same values of $K_F\lambda$ and η/λ (see tables 1 and 2). Hence, there is a unique inner microscale $2\pi/K_F \sim \lambda \sim \eta$, and in fact $2\pi/K_F$ is always equal to between λ and 2λ (see tables 1 and 2).

A second result is that, using this inner microscale and u'^2, the energy spectra of fractal-forced turbulence can be made to collapse for different Reynolds numbers as follows:

$$E(k) = u'^2 l f(kl), \tag{4.1}$$

where $f(kl)$ is a dimensionless function of kl which depends on β, and l is the inner microscale proportional to $2\pi/K_F$ and λ. In figure 8, we present an example of this

https://doi.org/10.1017/S0022112003007249 Published online by Cambridge University Press

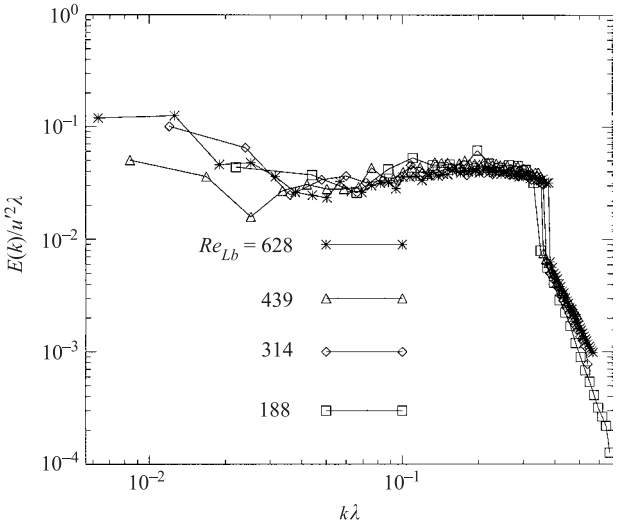


FIGURE 8. The energy spectrum compensated by $u'^2\lambda$ for different Reynolds numbers and for $\beta = 0.6$. For each value of β, the spectra collapse onto the functions shown in figure 4, for clarity we have shown only one value.

collapse for $\beta = 0.33$. The collapse is satisfactory for all wavenumbers smaller than K_F except at the very small wavenumbers where the statistical sample used to calculate $E(k)$ is in fact not sufficiently large.

This scaling (4.1) of the energy spectrum implies that the function $f(kl)$ cannot decrease faster than $(kl)^{-1}$ as k increases towards $K_F \sim 2\pi/l$, and indeed the spectra in figures 4 and 8 are much shallower than $(kl)^{-1}$. The reason is that $3u'^2/2$ must very closely equal $\int_{1/L_b}^{1/l} u'^2 l f(kl)\,\mathrm{d}k$ and be independent of l/L_b in the limit where $l/L_b \ll 1$.

This scaling (4.1) of the energy spectrum can also explain why $l \sim \lambda$. The dissipation rate is $\epsilon = 2\nu \int k^2 E(k)\,\mathrm{d}k \approx 2\nu \int_{1/L_b}^{1/l} k^2 u'^2 l f(kl)\,\mathrm{d}k$, which, in the limit $l/L_b \ll 1$, is proportional to $\nu u'^2/l^2$ provided that $f(kl)$ does not decrease faster than $(kl)^{-3}$ as k increases towards $K_F \sim 2\pi/l$. Since $f(kl)$ is in fact shallower than $(kl)^{-1}$ in our fractal-forced simulations, and because $\lambda^2 = 15\nu u'^2/\epsilon$ in homogeneous isotropic turbulence, we conclude that $l \sim \lambda$.

5. Energy transfer

Let us now consider the energy transfer relation for homogeneous isotropic and stationary (i.e. $(\partial/\partial t)E(k) = 0$) turbulence

$$\mathscr{F}(k) + T(k) = 2\nu k^2 E(k), \tag{5.1}$$

where $T(k)$ is the inter-scale energy transfer and $\mathscr{F}(k)$ is the energy input rate spectrum defined in (3.1) and plotted in figure 6. Examples of results obtained for $T(k)$ are given in figure 9. The inter-scale energy transfer is mostly negative in the forcing range $k \leqslant K_F$, indicating a loss of energy by nonlinear advection mechanisms, and positive beyond this range. The point where curves of different β values intersect in the energy and energy input spectra is also present in the $T(k)$ curves. In the range where $\mathscr{F}(k)$ is an increasing function of β, that is between the intersection point and K_F, Mazzi *et al.* (2002) have argued, on the basis of a GOY model of fractal forced turbulence, that $|T(k)| \sim k^{(3\beta-1)/2}$. Note that, in this range of wavenumbers in our DNS, $|T(k)|$

https://doi.org/10.1017/S0022112003007249 Published online by Cambridge University Press

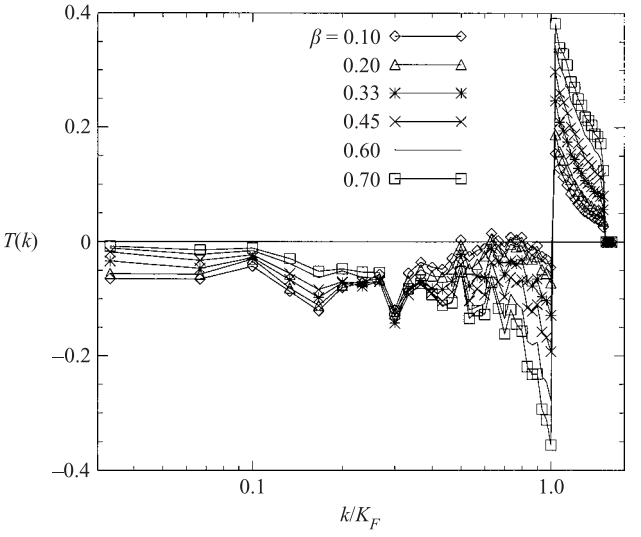


FIGURE 9. The transfer spectrum $T(k)$ for $N = 96$: K_F is the last forced wavenumber and the vertical line pair indicates the range of L for different values of β.

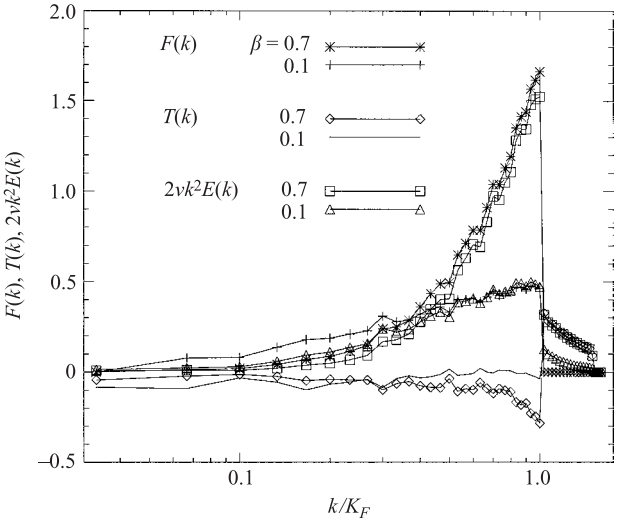


FIGURE 10. The terms of the energy transfer relation for $\beta = 0.7$ and $\beta = 0.1$.

appears to be a decreasing function of k for $\beta < 1/3$ with a steeper decrease for smaller values of β, and an increasing function of k for $\beta > 1/3$ with a steeper increase for larger values of β. This description is in good qualitative agreement with $|T(k)| \sim k^{(3\beta-1)/2}$.

In figure 10 we plot, for two different values of β, all the terms in the energy transfer relation, (5.1). We find that, in the fractal forcing range, $T(k)$ is small in magnitude and $\mathscr{F}(k) \approx 2\nu k^2 E(k)$, in contrast to RG theories (e.g. Frisch 1995) and the arguments of Mazzi *et al.* (2002). For $k > K_F$, where $\mathscr{F}(k) = 0$ by design, $T(k) = 2\nu k^2 E(k)$. The fact that more than 80% of the total dissipation occurs in the fractal forcing range (see tables 1 and 2) is consistent with the small values of $T(k)$ and $\mathscr{F}(k) \approx 2\nu k^2 E(k)$ in this range. An extended intermediate range of small scales, where $T(k)$ is very

https://doi.org/10.1017/S0022112003007249 Published online by Cambridge University Press

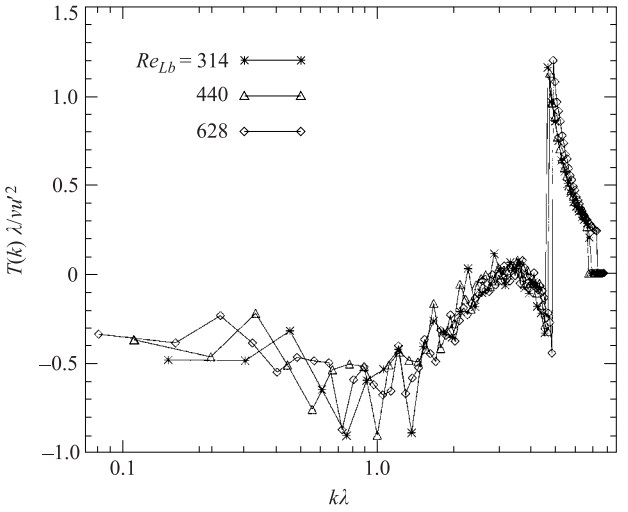


FIGURE 11. The transfer spectrum $T(k)$ compensated by $\nu u'^2\lambda^{-1}$ for different Reynolds numbers and for $\beta = 0.1$.

small or zero, is a property expected of equilibrium turbulence (forced at the large scales), only when the Reynolds number Re_{L_b} is extremely large, indeed very much larger than the Reynolds numbers currently achieved by DNS. The fractal forcing causes the turbulence to exhibit such a high-Reynolds-number property at moderate Reynolds number, but the range over which $T(k)$ is small is physically different from an inertial range because of the very large amount of dissipation that occurs in it.

If we substitute the scaling of the energy spectrum given by (4.1) into (5.1) we obtain

$$\mathscr{F}(k) + T(k) = 2\frac{\nu u'^2}{\lambda}(k\lambda)^2 f(k\lambda), \tag{5.2}$$

suggesting that

$$T(k) = \frac{\nu u'^2}{\lambda} g(k\lambda), \tag{5.3}$$

and

$$\mathscr{F}(k) = \frac{\nu u'^2}{\lambda} h(k\lambda), \tag{5.4}$$

under the constraint

$$g(k\lambda) + h(k\lambda) = 2(k\lambda)^2 f(k\lambda). \tag{5.5}$$

Figures 11 and 12 corroborate the scalings (5.3) and (5.4) (and similar figures were found for different values of β); in a way similar to figure 8, suitably scaled $T(k)$ and $\mathscr{F}(k)$ are plotted for different Reynolds numbers so as to display the collapse onto functions $g(k\lambda)$ and $h(k\lambda)$, respectively.

6. The energy dissipation rate ϵ

The dissipation rate ϵ and the Taylor microscale λ are related by $\epsilon = 15\nu u'^2/\lambda$. In our simulations of fractal forced turbulence, we increase the Reynolds number whilst

https://doi.org/10.1017/S0022112003007249 Published online by Cambridge University Press

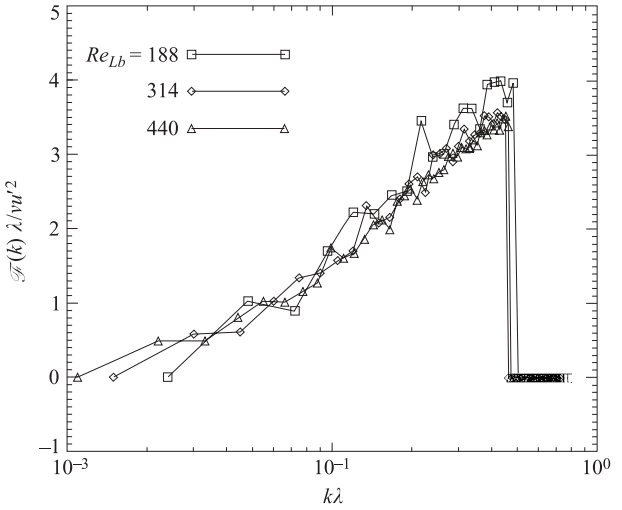


FIGURE 12. The energy input $\mathscr{F}(k)$ compensated by $\nu u'^2\lambda^{-1}$ for different Reynolds numbers and for $\beta = 0.1$.

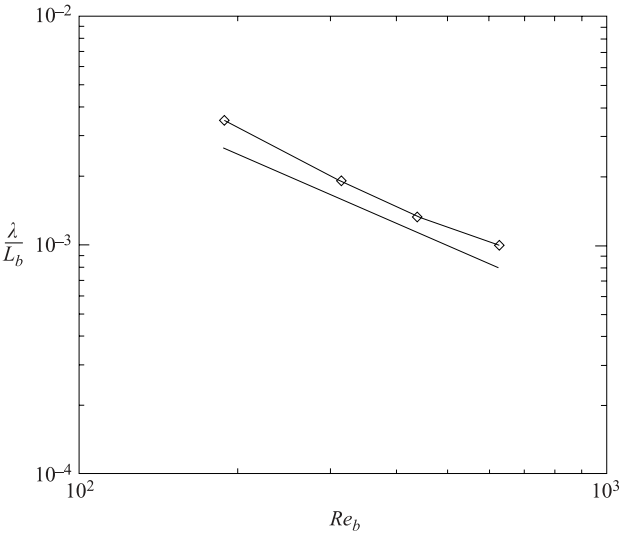


FIGURE 13. The scaling of λ with Reynolds number for $\beta = 0.33$, the straight line has slope -1.

keeping $K_F\eta$ constant, and find that

$$\lambda \sim L_b Re_{L_b}^{-1} \sim \frac{\nu}{u'}, \tag{6.1}$$

as shown in figure 13. This Reynolds number scaling is very different from the $Re_{L_b}^{-1/2}$ scaling of λ in homogeneous turbulence forced at the large scales only. It implies that $T(k) \sim u'^3 g(k\lambda)$ and $\mathscr{F}(k) \sim u'^3 h(k\lambda)$. It also implies that Re_λ is order 1 and that

$$\epsilon \sim \frac{u'^3}{L_b} Re_{L_b} \sim \frac{u'^3}{\lambda} \sim \frac{u'^4}{\nu} \tag{6.2}$$

https://doi.org/10.1017/S0022112003007249 Published online by Cambridge University Press

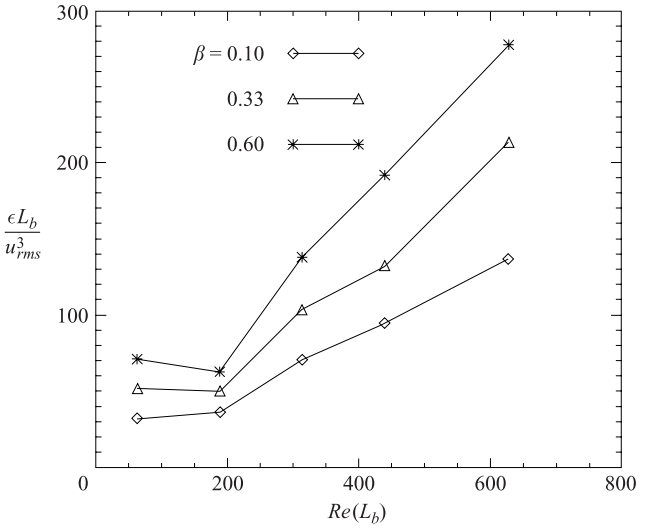


FIGURE 14. The non-dimensional dissipation rate $\epsilon L_b/u'^3$ as a function of Re_{L_b}.

as Re_{L_b} is increased whilst keeping $K_F\eta$ constant, a pair of conclusions that are corroborated by our DNS measurements (see tables 1 and 2 and figure 14). Note also that, from the scalings (6.1) and (6.2), $\eta \equiv (\nu^3/\epsilon)^{1/4} \sim \lambda$ as already observed in § 4 and tables 1 and 2. We have confirmed that our DNS lead to $\epsilon \sim u'^3/L_b$ as Re_{L_b} is increased whilst keeping $K_F L_b$ constant, but not $K_F\eta$.

7. Skewness and straining

In isotropic homogeneous turbulence, the velocity derivative skewness is related to the inter-scale energy transfer by (Batchelor 1953)

$$S = \left(\frac{135}{98}\right)^{1/2} \frac{\displaystyle\int_0^\infty k^2 T(k)\,\mathrm{d}k}{\left(\displaystyle\int_0^\infty k^2 E(k)\,\mathrm{d}k\right)^{3/2}} = \left(\frac{135}{98}\right)^{1/2} \left(\frac{2\nu}{\epsilon}\right)^{3/2} \int_0^\infty k^2 T(k)\,\mathrm{d}k. \qquad (7.1)$$

Using the scalings obtained in the previous sections, specifically $\epsilon \sim (u'^3/L_b)Re_{L_b}$, $T(k) = (\nu u'^2/\lambda)g(k\lambda)$ and $\lambda \sim L_b Re_{L_b}^{-1}$, it follows that S is independent of Re_{L_b}. In Kolmogorov equilibrium turbulence forced at the large scales, S is also independent of Reynolds number even though the scalings of ϵ, λ and $T(k)$ are different.

The relatively small values of S obtained in fractal forced turbulence compared with DNS turbulence forced only at the large scales (see tables 1 and 2) is consistent with the observed small magnitude of $T(k)$ in the fractal forcing range (see § 5). Another way to shed some light on the small values of S is by using Betchov's (1956) formula

$$S = -\frac{8}{105\langle(\partial u/\partial x)^2\rangle^{3/2}}\left[\langle\Lambda_1^3\rangle + \langle\Lambda_2^3\rangle + \langle\Lambda_3^3\rangle\right], \qquad (7.2)$$

where $\Lambda_1 \geqslant \Lambda_2 \geqslant \Lambda_3$ are the eigenvalues of the strain rate tensor S_{ij}. It is well known that $\Lambda_1 > 0$ and $\Lambda_3 < 0$ because of incompressibility. Similarly to turbulence forced at the large scales, we find that $\langle\Lambda_2^3\rangle$ is positive. As argued by Tsinober (2000) and

https://doi.org/10.1017/S0022112003007249 Published online by Cambridge University Press

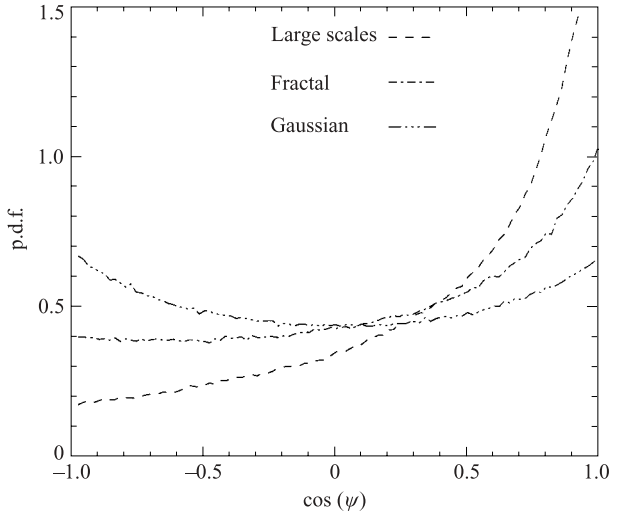


FIGURE 15. The p.d.f. of the cosine of the angle between the vorticity vector and the vortex stretching vector $\boldsymbol{W}$, for $\beta = 0.1$. There is no significant difference with corresponding plots for other values of β.

Betchov (1956), the non-linear inter-scale energy transfer is directly associated with compression of fluid elements because $\langle \Lambda_3^3 \rangle$ dominates S, and the sign of S reflects the sign of $\langle \Lambda_3^3 \rangle$. In our fractal forced turbulence we find (with very little variation with β and Reynolds number)

$$\langle \Lambda_1^3 \rangle \approx 6.4 \left\langle \left(\frac{\partial u}{\partial x} \right)^2 \right\rangle^{3/2}, \quad \langle \Lambda_2^3 \rangle \approx 0.2 \left\langle \left(\frac{\partial u}{\partial x} \right)^2 \right\rangle^{3/2}, \quad \langle \Lambda_2^3 \rangle \approx -10 \left\langle \left(\frac{\partial u}{\partial x} \right)^2 \right\rangle^{3/2}.$$

In turbulence forced only at the large scales (runs XIV and XV), $\langle \Lambda_1^3 \rangle$ is about the same, $\langle \Lambda_2^3 \rangle$ is about double and $\langle \Lambda_2^3 \rangle \approx -13.5 \langle (\partial u/\partial x)^2 \rangle^{3/2}$. We see, therefore, that the small magnitudes of $T(k)$ observed in the fractal forcing range are accompanied by a significant reduction of local compression which is responsible for the lower values of S.

We have also calculated the alignment statistics of the vorticity vector $\boldsymbol{\omega}$ with the eigenvectors $\boldsymbol{e}_i$ ($i = 1, 2, 3$ corresponding to Λ_i) of the rate of strain tensor S_{ij} and with the vortex stretching vector $W_i = \omega_j S_{ij}$ (Shtilman, Spector & Tsinober 1993). The p.d.f. of the cosine of the angle between $\boldsymbol{\omega}$ and $\boldsymbol{W}$ is shown in figure 15. Qualitatively, the alignment remains as in turbulence forced at the large scales (Shtilman *et al.* 1993), but quantitatively this alignment is weaker.

The probability density functions (p.d.f.s) of $\cos \psi_i$, where ψ_i is the angle between the vorticity vector and $\boldsymbol{e}_i$, are qualitatively similar to those published in the literature for turbulence forced only at the large scales (e.g. Ashurst *et al.* 1987) and we therefore omit them here. However, there is a quantitative difference in the variances of these p.d.f.s (figure 16) which are found to be all closer to 1/3 than in turbulence forced at the large scales (see She, Jackson & Orszag 1991). The value 1/3 corresponds to random angles and therefore to no preferred alignment. As in turbulence forced at the large scales, the vorticity is preferentially aligned with $\boldsymbol{e}_2$ with some tendency to be normal to $\boldsymbol{e}_3$. However, these alignments are significantly less marked than in turbulence forced at the large scales.

https://doi.org/10.1017/S0022112003007249 Published online by Cambridge University Press

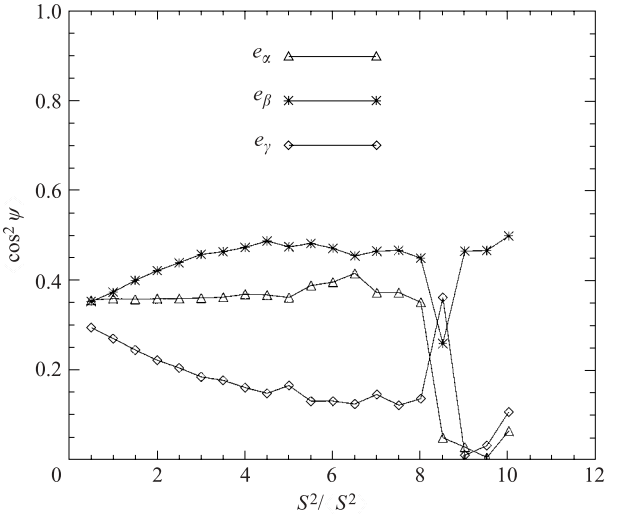


FIGURE 16. A plot of $\langle\cos^2(\psi)\rangle$ for the three eigenvectors as a function of strain for $\beta = 0.1$.There is no significant difference with corresponding plots for other values of β.

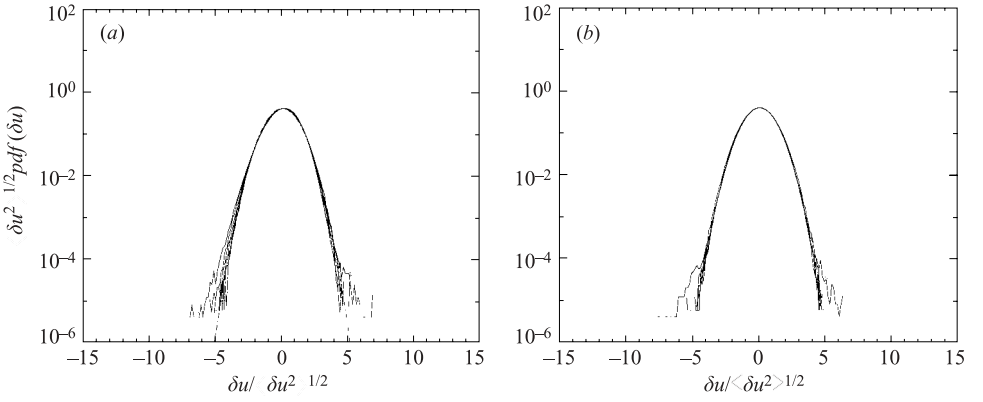


FIGURE 17. The plot of the compensated $pdf(\delta u_r)$ for several values of r for run IX, $\beta = 0.7$, for (a) a flow forced with a fully scale invariant forcing and (b) a similar flow with random phases. There is no significant difference with corresponding plots obtained for other values of β.

8. Probability density functions of velocity increments

We have calculated the p.d.f.s $pdf(\delta u_r)$ of longitudinal velocity increments $\delta u_r = (\boldsymbol{u}(\boldsymbol{x}+\boldsymbol{r}) - \boldsymbol{u}(\boldsymbol{x}))\cdot\boldsymbol{r}/|\boldsymbol{r}|$, for several values of $r = |\boldsymbol{r}|$, ranging from about 2η to about four times the value of the integral length scale L. In figure 17(a), we plot $\langle\delta u^2\rangle^{1/2} pdf(\delta u_r)$ versus $\delta u/\langle\delta u^2\rangle^{1/2}$. The dashed line is the corresponding Gaussian. It is striking that $pdf(\delta u_r)$ is approximated well by the Gaussian form for all our values of r. In turbulence forced at the large scales only, $pdf(\delta u_r)$ is increasingly non-Gaussian for increasingly small scales.

These results concur with the relatively low values of S and F in our fractal forced turbulence (see tables 1 and 2) and the weakened tendencies of alignment of $\boldsymbol{\omega}$ with $\boldsymbol{W}$ and the eigenvectors of the strain rate tensor. Shtilman *et al.* (1993) have, in fact, shown that these alignments disappear completely when the Fourier phases of the

https://doi.org/10.1017/S0022112003007249 Published online by Cambridge University Press

Run	N	β	$K_F L_b$	$k_{max} L_b$	$\sigma = 1/R$	Re_{L_b}
I	96	0.1	169.6	282.6	1.94	314
II	64	0.33	119.3	188.4	1.81	188
III	128	0.6	257.5	376.8	1.70	440
IV	192	0.2	276.3	565.2	1.88	628
V	192	0.45	326.6	565.2	1.76	628
VI	192	0.75	332.9	565.2	1.66	628
VII	192	0.6	351.7	565.2	1.95	628
VIII	192	0.6	370.5	565.2	1.22	628
IX	192	0.6	376.8	565.2	1.05	628
X	192	0.6	370.5	565.2	1.03	628

TABLE 3. DNS parameters and data: discretely self-similar forcing.

turbulence are randomized and the turbulence is made Gaussian with the same energy spectrum. They do not disappear here, but are weakened, and do indeed disappear when we randomize the Fourier phases of our fractal forced turbulence (see example given in figure 15), in which case $pdf(\delta u_r)$ becomes exactly Gaussian (figure 17*b*).

In conclusion, our fractal forced turbulence is not exactly Gaussian as its Fourier phases are not random and the geometrical alignments mentioned above do not disappear but are weakened in comparison to turbulence forced at the large scales. The p.d.f.s of δu_r are, however, close to, though not exactly, Gaussian, and the small discrepancy from Gaussianity accounts for the survival of the geometrical alignments.

9. Fractal forcing with discrete self-similarity

We close this investigation with a few DNS runs where the fractal forcing is not fully, but only discretely, self-similar according to (2.14). Such fractal forcing depends on two parameters, β and σ, which correspond, respectively, to the parameters D_f (fractal dimension) and R (scale ratio between successive iterations of the fractal construction, $R < 1$) of fractal objects such as in figure 1): $\sigma = 1/R$ and β is sufficiently well approximated by, though in practice smaller than, $D_f - 2$ (see Queiros-Conde & Vassilicos 2001; Mazzi *et al.* 2002). In general, the parameters β and σ (equivalently D_f and R) are independent, but for a given fractal construction (for example that in figure 1) they are not. In the case of figure 1, $\beta = -((\ln(8)/\ln(1/\sigma)) + 2)$, and in the case of a two-dimensional version of that figure, $\beta = -((\ln(4)/\ln(1/\sigma)) + 2)$ (see Queiros-Conde & Vassilicos 2001; Mazzi *et al.* 2002).

In table 3, we give the parameters characterizing the DNS performed with discretely self-similar forcing and in figures 18 and 19, we present energy spectra obtained from these simulations. In figure 18, β and σ are varied together according to $\beta = -((\ln(4)/\ln(1/\sigma)) + 2)$ and in figure 19, β is kept constant whilst σ is decreased from 1.95 to 1.03. These results indicate dynamics different from those studied in the bulk of the present paper, although the flow remains stationary, isotropic and homogeneous. The energy spectra appear as combinations of two coexisting spectral forms, one continuous and decreasing, the other spiky. These spikes are positioned at the forced wavenumbers. As β increases and more energy is injected into smaller scales by the forcing, the magnitude of these spikes changes from being a decreasing to an increasing function of wavenumber (see figure 18). Also, σ decreases as a consequence of increasing β, and therefore the number of spikes increases too, as indeed is seen in figure 18.

https://doi.org/10.1017/S0022112003007249 Published online by Cambridge University Press

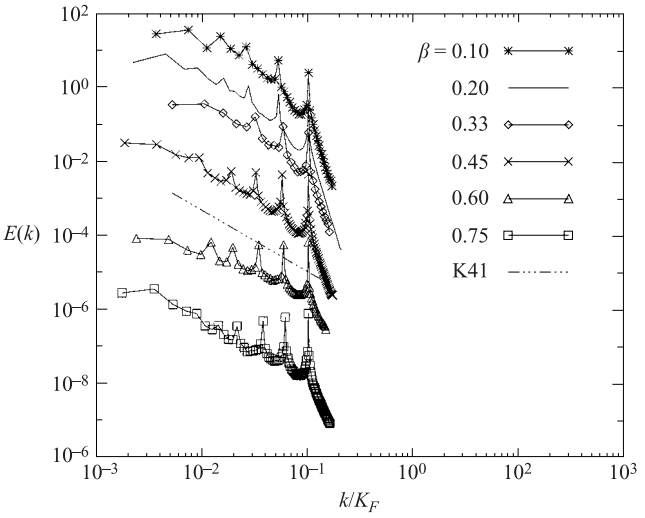


FIGURE 18. The energy spectrum for different values of β. β and R are varied dependently.

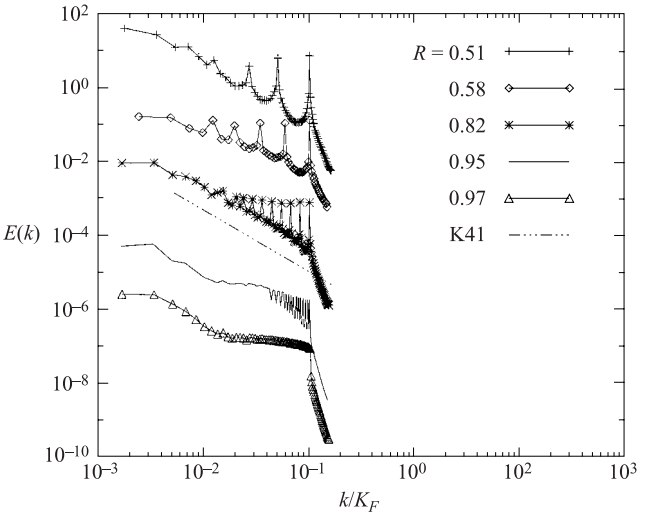


FIGURE 19. The energy spectrum for different values of R and $\beta = 0.6$.

When β is kept constant and σ is decreased towards 1, the spikes gradually dominate the energy spectrum and lead to a shape similar to that observed in our previous sections (see figure 19). In the limit $\sigma \to 1$, the fractal forcing changes from being discretely to being fully self-similar, and the energy spectrum changes from exhibiting the dual behaviour of figure 18 to the nearly constant and continuous spectrum of figure 4.

10. Conclusion

Our DNS study suggests that it is possible to modify some central properties of turbulence by forcing it in some fractal way. The relation of the turbulent kinetic energy dissipation ϵ to the Reynolds number is dramatically modified and so are the

https://doi.org/10.1017/S0022112003007249 Published online by Cambridge University Press

p.d.f.s of longitudinal velocity increments which are approximately Gaussian at all scales, even the smallest ones around η.

Fractal forced turbulence at moderate to small Reynolds numbers (referring to Reynolds numbers tried here $Re_{L_b} < 650$) exhibits some properties which turbulence forced at the large scales displays only at very high Reynolds numbers (beyond the current reach of DNS): small-scale isotropy is defined unusually well (for DNS turbulence) and the interscale energy transfer is negligible in the fractal forcing range of scales. However, this range is not the classical inertial range; more than 80% of the total dissipation occurs in the fractal forcing range and we also find that $\epsilon \sim (u'^3/L_b)Re_{L_b} \sim u'^3/\lambda$ rather than $\epsilon \sim u'^3/L_b$. Also, the Taylor microscale is pegged to the inner length scale $2\pi/K_F$ of the fractal forcing range and the energy spectrum is much shallower than $k^{-5/3}$; fractal dimensions D_f of the fractal stirrer lead to more energy at higher wavenumbers of the spectrum. This last result is similar to corresponding conclusions obtained using renormalization group methods (RG). Moreover, Sain *et al.* (1998) found a critical value for the forcing spectrum exponent above which the energy spectrum takes a Kolmogorov shape. This is not confirmed in our simulations (as opposed to the GOY model simulations of Mazzi *et al.* (2002) where it was), but we do confirm that L decreases with increasing steepness of the forcing spectrum. We should note, however, that unlike the forcing used in RG calculations, ours is not delta-correlated in time.

More laboratory experiments on fractal forced turbulence are needed. In the wind-tunnel experiments of Queiros-Conde & Vassilicos (2001) and Staicu *et al.* (2003), the turbulence is generated by fractal grids and then convected away, whereas in the present DNS, the turbulence is constantly subjected to fractal forcing inside a periodic box. This paper's DNS results might therefore be more favourably compared with results from a laboratory experiment on confined turbulence subjected to some form of persistent fractal stirring.

The fractal grids used by Queiros-Conde & Vassilicos (2001) and Staicu *et al.* (2003) are discretely self-similar. Further research is therefore required on DNS turbulence forced by a fractal forcing with discrete self-similarity.

We would like to thank Professor K. R. Sreenivasan for inviting B. M. to spend the period July–August 2001 at the Department of Mechanical Engineering, Yale University where some of the work reported in this paper was carried out. B. M. acknowledges the Cambridge Philosophical Society for the relevant travel grant. Some of the work was also carried out during the Summer School on Environmental Fluid Mechanics held in July 2002 at the Universitat Politecnica de Catalunya where J. C. V. was Cluster Professor. B. M. acknowledges a grant which enabled him to attend this summer school. J. C. V. acknowledges support from the Royal Society.

Appendix. The forcing of a fractal stirrer

The construction of the Koch pole (see figure 20) is based on that of the Koch curve (see Mandelbrot 1977). The pole is made of thin blades of length L_n $(0 < n < n_{max})$ and width $\omega \ll L_{n_{max}}$. The blades are placed such that their area $L_n\omega$ is normal to a uniform incoming flow so that the drag force is proportional to $L_n\omega$ for each blade. The thickness of each blade is assumed to be even smaller than ω and small enough to allow the neglect of the skin friction contribution to the drag.

The total drag force experienced by the Koch pole and with which the Koch pole generates the turbulence in its wake if held fixed is proportional to the sum of the

https://doi.org/10.1017/S0022112003007249 Published online by Cambridge University Press

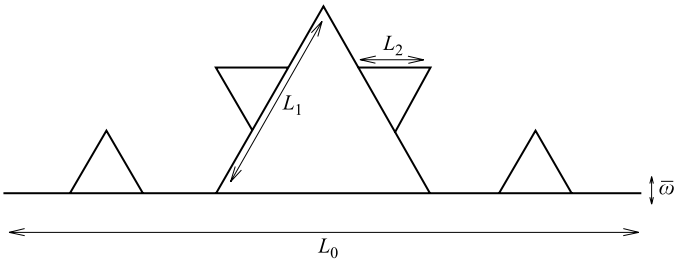


FIGURE 20. Sketch of the Koch pole.

following contributions: $f_0 = L_0\omega$ for the one blade of length L_0, $f_1 = 2L_1\omega$ for the two blades of length L_1, $f_2 = 8L_2\omega$ for the 8 blades of length L_2, etc. In general, $f_n = N_n L_n \omega$ where N_n is the number of blades of length L_n and $N_n = 4^n/2$ for $n \geqslant 1$ in the case of the Koch pole where $L_n = 3^{-n}L_0$ for $n \geqslant 1$. It follows that $2N_n = (L_n/L_0)^{-D_f}$ where $D_f = \ln 4/\ln 3$ is the fractal dimension of the Koch curve (Mandelbrot 1977) and $f_n = (\omega L_0/2)(L_n/L_0)^{1-D_f}$. The Fourier representation of this forcing at wavenumber $k_n \sim 1/L_n$ might therefore be expected to have an amplitude proportional to $k_n^{D_f-1}$.

More general fractal poles can be thought of where $L_n = (1/\delta)^n L_0$ with $\delta > 1$ and $2N_n = M^n$ where $M > \delta$. The fractal dimension of such fractal poles is $D_f = \ln M/\ln \delta$ and the force at wavenumber k_n is proportional to k_n^β where $\beta > 0$ because $\beta = D_f - 1$ and $D_f > 1$.

REFERENCES

ASHURST, WM. T., KERNSTEIN, A. R., KERR, R. M. & GIBSON, C. H. 1987 The alignment of vorticity and scalar gradient with strain rate simulated Navier–Stokes turbulence. *Phys. Fluids* **30**, 2343–2353.

BATCHELOR, G. K. 1953 *The Theory of Homogenous Turbulence*. Cambridge University Press.

BETCHOV, R. 1956 An inequality concerning production of vorticity in turbulence. *J. Fluid Mech.* **1**, 497–504.

ESWARAN, V. & POPE, S. B. 1988 Direct numerical simulations of the turbulent mixing of a passive scalar. *Phys. Fluids* **31**, 506–520.

FLOHR, P. 1999 Small-scale flow structure in turbulence: fundamentals and numerical models. PhD thesis, University of Cambridge.

FRISCH, U. 1995 *Turbulence: The Legacy of A. N. Kolmogorov*. Cambridge University Press.

FRISCH, U., SULEM, P. L. & NELKIN, M. 1978 A simple dynamical model of intermittent fully developed turbulence. *J. Fluid Mech.* **87**, 719–736.

HUNT, J. C. R. & VASSILICOS, J. C. 1991 Kolmogorov's contribution to the physical and geometrical understanding of turbulent flows and recent developments. *Proc. R. Soc. Lond.* A **434**, 183–210.

JIMÉNEZ, J., WRAY, A. A., SAFFMAN, P. G. & ROGALLO. R. S. 1993 The structure of intense vorticity in isotropic turbulence. *J. Fluid Mech.* **255**, 65–90.

KERR, R. M. 1985 Higher-order derivative correlations and the alignment of small-scale structures in isotropic numerical turbulence. *J. Fluid Mech.* **153**, 31–58.

LESIEUR, M. 1990 *Turbulence in Fluids*. Kluwer.

LUNDGREN, T. S. 1982 Strained spiral vortex model for turbulent fine structure. *Phys. Fluids* **25**, 2193.

MCCOMB, W. D. 1990 *The Physics of Fluid Turbulence*. Clarendon.

MANDELBROT, B. 1974 Intermittent turbulence in self-similar cascades: divergence of high moments and dimension of the carrier. *J. Fluid Mech.* **62**, 331–358.

MANDELBROT, B. 1977 *Fractals: Form, Chance and Dimension*. Freeman, San Francisco.

MAZZI, B., OKKELS, F. & VASSILICOS, J. C. 2002 A shell model approach to fractal induced turbulence. *Eur. Phys. J.* B **28**, 243–251.

https://doi.org/10.1017/S0022112003007249 Published online by Cambridge University Press

Novikov, E. A. 1970 *Prikl. Math. Mekh.* **35**, 266–277.

Onsager, L. 1949 Statistical hydrodynamics. *Nuovo Cimento (Suppl.)* **6**, 279.

Parisi, G. & Frisch, U. 1985 A multifractal model of intermittency. In *Turbulence and predictability in geophysical fluid dynamics and climate dynamics* (ed. M. Ghil, R. Benzi & G. Parisi) pp. 84–88. North-Holland.

Perry, A. E., Henbest, S. & Chong, M. S. 1986 A theoretical and experimental study of wall turbulence. *J. Fluid Mech.* **165**, 139–199.

Queiros-Conde, D. & Vassilicos, J. C. 2001 Turbulent wakes of 3-D fractal grids. In *Intermittency in turbulence flows* (ed. J. C. Vassilicos). Cambridge University Press.

Sain, A., Pandit, M. & Pandit, R. 1998 Turbulence and multiscaling in the randomly forced Navier–Stokes equations. *Phys. Rev. Lett.* **81**, 4377.

She, Z.-S., Jackson, E. & Orszag, S. 1991 Structure and dynamics of homogenous turbulence: models and simulations. *Proc. R. Soc.* **434**, 101–124.

Shtilman, M., Spector, M. & Tsinober, A. 1993 On some kinematic versus dynamic properties of homogenous turbulence. *J. Fluid Mech.* **247**, 65–77.

Smith, L. M. & Woodruff S. L. 1998 Renormalization-group analysis of turbulence. *Annu. Rev. Fluid Mech.* **30**, 275–310.

Staicu, A., Mazzi, B., Vassilicos, J. C. & Water, W. van der 2003 Turbulent wakes of fractal objects. *Phys. Rev.* E **67**, 066306.

Tsinober, A. 2000 Vortex stretching versus production of strain/dissipation. In *Turbulence Structure and Vortex Dynamics* (ed. J. C. R. Hunt & J. C. Vassilicos), pp. 164–191. Cambridge University Press.

Vassilicos, J. C. 1992 The multispiral model of turbulence and intermittency. In *Topological Aspects of the Dynamics of Fluids and Plasmas* (ed. H. K. Moffatt, G. M. Zaslavsky, P. Comte & M. Tabor), pp. 427–442. Kluwer.

Vassilicos, J. C. & Hunt, J. C. R. 1991 Fractal dimension and spectra of interfaces with application to turbulence. *Proc. R. Soc. Lond.* A **435**, 505–534.

https://doi.org/10.1017/S0022112003007249 Published online by Cambridge University Press